Transition energies of antiprotonic atoms

Antons Nikolajevs
Supervisors: Malgorzata Grosbart, Fredrik Parnefjord Gustafsson, Michael Doser

Abstract
One of the proposed experiments at AEgIS concerns the spectroscopic study of antiproton bound system of medium and heavy nuclei. In this work the antiprotonic atom transition energies are calculated for the elements of interest and the infuence of different corrections are explored, such as finite-size effect, vacuum polarization and strong interaction shift. As the antiprotonic atoms will be formed in high magnetic field, splitting due to Zeeman effect was compared to transition energies for different principal quantum numbers. In order to understand the deepest quantum level available for spectroscopic study, the overlap of the antiproton wave function with the nucleus is calculated.

Keywords
Antiprotons; finite-size effect; vacuum polarization; strong interaction shift; Zeeman effect; transition rate; annihilation rate.

1 Introduction

When antiprotons are stopped in matter, they can replace one of the outer shell electrons, thus creating an antiprotonic atom. After the capture, antiproton starts to deexcite by Auger process, radiative transitions and annihilation [1]. Auger process dominates at states with large principal quantum number n [2]. After all electrons are expelled, deexcitation happens through radiative transitions. At states with smaller principal quantum number n, energy level shift due to strong interaction occur which results in shift of transition energy [3]. Other effects, such as relativistic effect, vacuum polarization and finite size effect, can also change transition energy [4].

As the AEgIS collaboration plan to produce antiprotonic atoms [5], it is important to estimate the expected transition energies of the antiprotonic atoms proposed for study at AEgIS.

As the antiprotonic atoms will be formed in high magnetic field $B \approx 5$ T, it is important to compare Zeeman splitting to transition energy with between energy levels with large principal quantum number n (Rydberg states).

Antiprotonic bound systems provide an excellent benchmark for high field QED and study of nuclei.

2 Calculations

2.1 Energy levels and transition energies

The most simple model that can describe antiprotonic atoms is the Bohr model. Energy levels of the antiproton are given by[3]:

$$E_n = -\frac{\mu Z^2}{2n^2} \tag{1}$$

Where μ is reduced mass of the antiproton, which accounts for the mass shift [6], Z is the nuclear charge and n is the principal quantum number. Using the above equation it is possible to estimate transition energies of the antiproton as a difference between different energy values.

The Bohr's model does not account for relativistic effects therefore energy values given by the Dirac equation are preferred:

$$E_{Nj} = \frac{1}{\alpha^2\sqrt{1+(\frac{\alpha Z}{N+\mu})^2 s}}, \tag{2}$$

where $\nu = \sqrt{(j+1/2)^2 - (\alpha Z)^2}$ and $N = n - j - 1/2$. The Dirac equation removes the degeneracy of levels with the same total angular momentum j.

A more precise formula for energy levels of antiprotonic atoms which includes vacuum polarization and relativistic effects is [2]:

$$E = E_n \left\{ 1 + \left(\frac{Z\alpha}{n}\right)^2 \cdot \left[\frac{\mu}{4M} - \frac{3}{4} + \frac{n}{l+1/2}(1 + a_{vp} + a_{lj}) \right] \right\}. \tag{3}$$

In the equation above $a_{lj} = (l-j)/(l+1/2)$. And the vacuum polarization is calculated based on [7] as follows:

$$a_{vp} = \frac{2n(2l+1)}{3\pi Z^2 \alpha} \int_1^\infty (1 + nZ\alpha\mu t)^{-2n} t^{-2} \sqrt{t^2-1}(1 + 1/2t^2) dt \tag{4}$$

Where E_n is calculated using equation 1.

As protons and neutrons are distributed inside the nucleus, the point charge approximation is not sufficient for energy level calculations. This results in a difference between calculated energies and experimentally observed energies - the finite size effect. The finite size effect can be treated as a small perturbation [4]:

$$E_{FS} = \langle R_{nl} | \phi(r) - Z/r | R_{nl} \rangle = \int_0^\infty (\phi - Z/r) |R_{nl}|^2 r^2 dr, \tag{5}$$

where $\phi(r)$ is the potential produced by the finite charge distribution and $R_{nl}(r)$ is the radial wave function.

Potential ϕ can be calculated as:

$$\phi(r) = \frac{1}{r}\int_0^r \rho(t) t^2 dt + \int_r^\infty \rho(t) t dt. \tag{6}$$

Figure 1 shows potential due to point charge and potential due to continuous charge distribution. As can be seen, potential due to charge distribution is finite at $r = 0$ while point charge potential is infinite. This results in lower bound state energies as the electrostatic attraction is smaller for finite charge distribution.

To calculate the potential in equation 6 charge distribution is needed. In many cases Fermi distribution is assumed for both neutrons and protons [8]:

$$\rho(r) = \frac{\rho_0}{1 + \exp\left(\frac{(r-c)}{t} 4\ln(3)\right)}. \tag{7}$$

Here c is half-density radius and t is the skin thickness. Values $c = 1.1 \cdot A^{1/3}$ fm and $t = 2.5$ fm are assumed. Each density is normalized as follows:

$$\int_0^r \rho_A(r) r^2 dr = A. \tag{8}$$

An example of density distribution is shown in figure 2.

At lower levels strong interaction becomes significant compared to electrostatic interaction, therefore strong interaction shift of the energy levels should be considered. In many cases interaction potential is assumed to be [9]:

$$V_{st} = -\frac{2\pi}{\mu}\left(1 + \frac{\mu}{M}\right)\left[A_1\rho_n + \frac{1}{2}(A_1 + A_0)\rho_p\right] \tag{9}$$

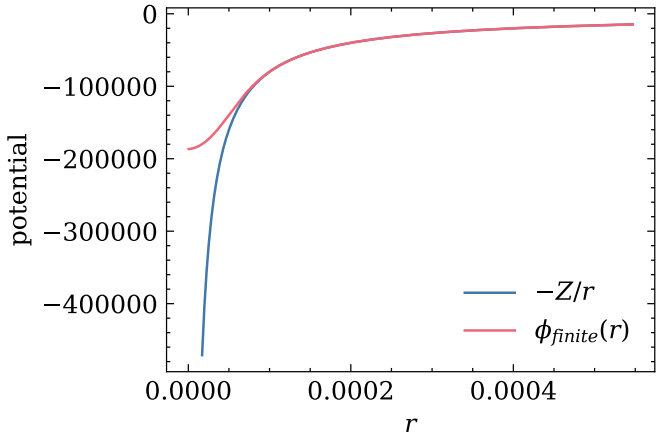

Figure 1: Potentials due to point charge (blue curve) and finite charge distribution (red curve) for ^{16}O. Charge distribution was assumed to have form given in equation 7.

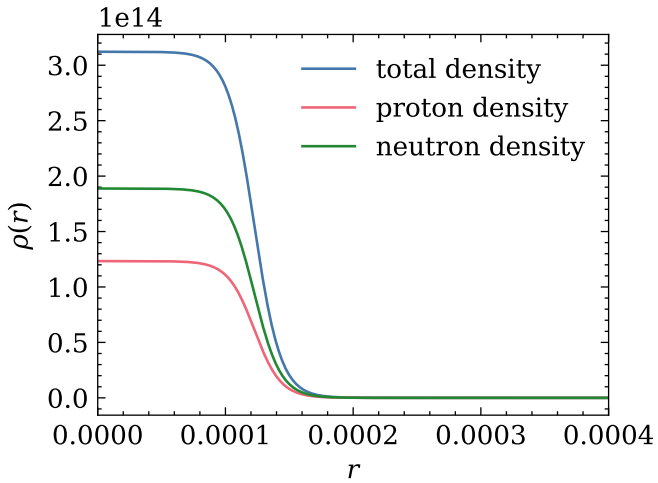

Figure 2: Assumed density distribution for neutrons and protons inside the thallium nucleus (A=201, Z=81), as well as total nuclear density.

where A_0 and A_1 are effective scattering lengths which vales are taken as $A_0 = [-1.16 + i0.86]$ fm and $A_1 = [-0.63 + i0.63]$ fm [10] and M is the mass of the nucleus.

As there are many uncertainties in the shape of neutron distribution as well as due to limited precision of scattering lengths, potential 9 is reduced to a simpler form [11]:

$$V_{st} = -\frac{1\pi}{\mu}\left(1 + \frac{\mu}{M}\right)\overline{a}\rho(r), \tag{10}$$

where $\overline{a}$ is an averaged effective scattering length and $\rho(r) = \rho_Z(r) + \rho_N(r)$ is total nuclear density.

Similarly to the finite size effect, strong interaction energy shift is treated perturbatively:

$$E_{Str} = \langle R_{nl}|V_{st}|R_{nl}\rangle = \int_0^r V_{st}(r)|R_{nl}(r)|^2 r^2 dr. \tag{11}$$

As the potential is proportional to the nuclear density, the energy shift due to strong interaction is also proportional to the overlap of antiprotonic wave function with nuclear density.

A comparison between potential 9 and 10 was made by comparing estimated energy shifts to the reported shifts in [4]. The comparison results are shown in figure 3. In the comparison value for $\overline{a} =$

transition	E_{bohr}	E_{dirac}	E_{vp}	E_{st}	E_{finite}	E_{tot}	E_{exp}, [13]
$10 \rightarrow 9$	382.61	383.81	385.87	0.015	-0.0020	385.88	386.05 ± 0.17

Table 1: Energy for the $10 \rightarrow 9$ transition in thallium. Energies are given in keV. Total energy is calculated as $E_{vp} + E_{st} + E_{finite}$, where E_{vp} is calculated using equation 3

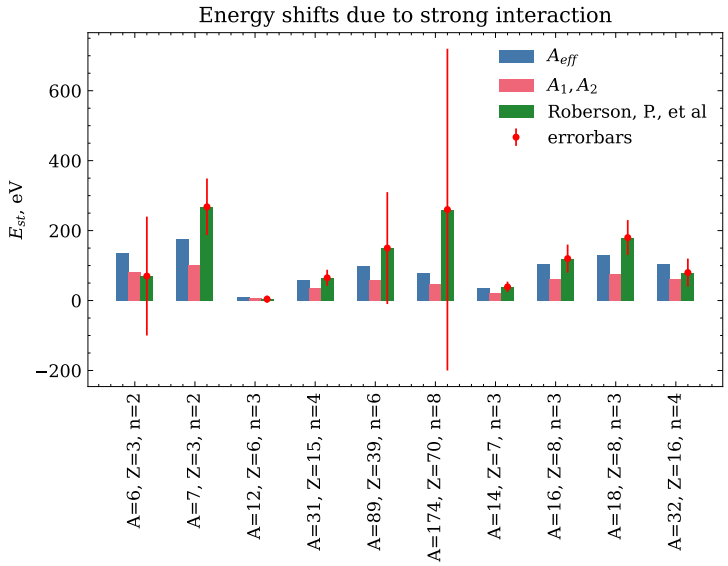

Figure 3: Comparison of potential in equation 9 (red bars) and equation 10 (blue bars) to experimental data taken from [4] (green bars) for different atoms.

$[1.53 + i2.50]$ fm was taken from [12]. It can be seen that potential (see eq. 10) describes experimental data better and it will be used in other calculations.

Described corrections to transition energies were compared to experimental data taken from [13] (see tab. 1). Total energy with finite-size correction and strong interaction shift equals to experimentally observed transition energy within reported experimental error.

2.2 Annihilation probability

Three main deexcitation processes are Auger transitions, radiative transitions and annihilation on the nucleus [14].

Auger process dominates in the upper part of the cascade while radiative transitions take over at lower energy levels [2]. In case when all electrons are expelled from the antiprotonic atom, Auger process can no longer happen, therefore the only deexcitation processes possible are radiative transition and annihilation.

Radiative transition rate for dipole transitions is given by [14, 15]:

$$\Gamma^{rad}_{n_1 l_1 \rightarrow n_2 l_2} = \frac{4e^2}{3\hbar^4 c^3} \left(\frac{a_0}{\mu Z} \right)^2 (\Delta E_{n_1 n_2})^3 \frac{\max(l_1, l_2)}{2l_1 + 1} \int_0^r R_{n_1 l_1}(r) R_{n_2 l_2}(r) r^3 dr. \tag{12}$$

As the antiproton reaches lower energy levels, its wave function overlap with a nucleus becomes larger. The antiproton radial distribution of absorption probability is proportional to the overlap of the wave function and nucleus [16]:

$$P_{nl}(r) = \rho(r) |R_{nl}(r)|^2 r^2 \tag{13}$$

The total overlap of the antiprotonic wave function and a nucleus can be estimated by integrating

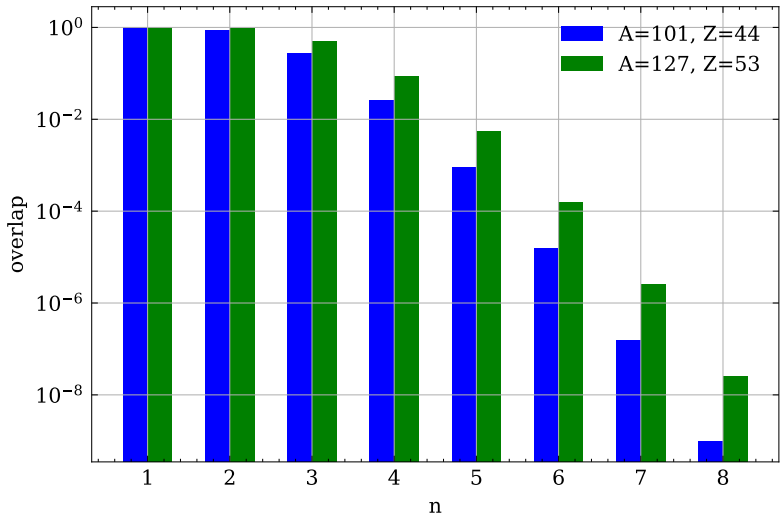

Figure 4: Wave function overlap with nucleus for different circular states for iodine (A=127, Z=53) and ruthenium (A=101, Z=44).

equation 13:

$$\text{overlap} = \int_0^\infty \rho(r)|R_{nl}(r)|^2 r^2 dr. \tag{14}$$

Note, that nuclear density used in equation 14 is not normalized i.e. $\rho(r << c) = 1$ and $\rho(r >> c) = 0$.

Described overlaps were calculated for Iodine (A=127, Z=53) and Ruthenium (A=101, Z=44) for circular states only ($l = n - 1$ states). Results are shows in figure 4. The last observed transition in iodine is $n = 8 \rightarrow n = 7$ [9], which means that at $n = 7$ antiproton annihilation occurs. The overlap at $n = 7$ for iodine is $2.5 \cdot 10^{-6}$. This allows for estimation of the last transition in ruthenium by finding state with similar overlap. The state with similar overlap is $n = 6$ with an overlap of $1.505 \cdot 10^{-5}$, which means that the last transition can be expected to be $n = 7 \rightarrow = 6$.

In figure 5 overlap for different (n, l) states is shown. It can be seen, that overlap for circular states is much smaller than for other states which results in smaller annihilation probability. It can also be seen that for atoms with smaller atomic number the overlap is also smaller.

As the dominating processes for low n levels are radiative transition and annihilation, the last observable transition can be estimated bu taking the ratio of annihilation rate and transition rate.

The annihilation rate is given by [14, 17]:

$$\Gamma^{cap}_{n_1 l_1} = \frac{2}{\hbar} \int_0^\infty \text{Im}\{V_{st}(r)\}|R_{n_1 l_1}(r)|^2 r^2 dr \tag{15}$$

Therefore an annihilation is expected when capture rate for n-th state is significantly larger than radiative transition rate from n-th state to $n - 1$, i.e. $\Gamma^{cap}_{n,n-1}/\Gamma^{rad}_{(n,n-1)\rightarrow(n-1,n-2)} >> 1$.

2.3 Zeeman splitting

As the measurements will to be performed in a strong magnetic field, Zeeman splitting may become comparable or even greater than splitting between E_n energy levels for Rydberg states.

As the field is in the order of 1 T, the strong field approximation can be used for such calculations. For an unperturbed antiprotonic atom in a circular state (n, $l = n - 1$) all $2l + 1 = 2n - 1$ magnetic sublevels are degenerate. In an external magnetic field the degeneracy is removed and each magnetic sublevel acquires additional energy:

$$E_Z = (g_{\bar{p}} m_s + m_l)\mu_B B, \tag{16}$$

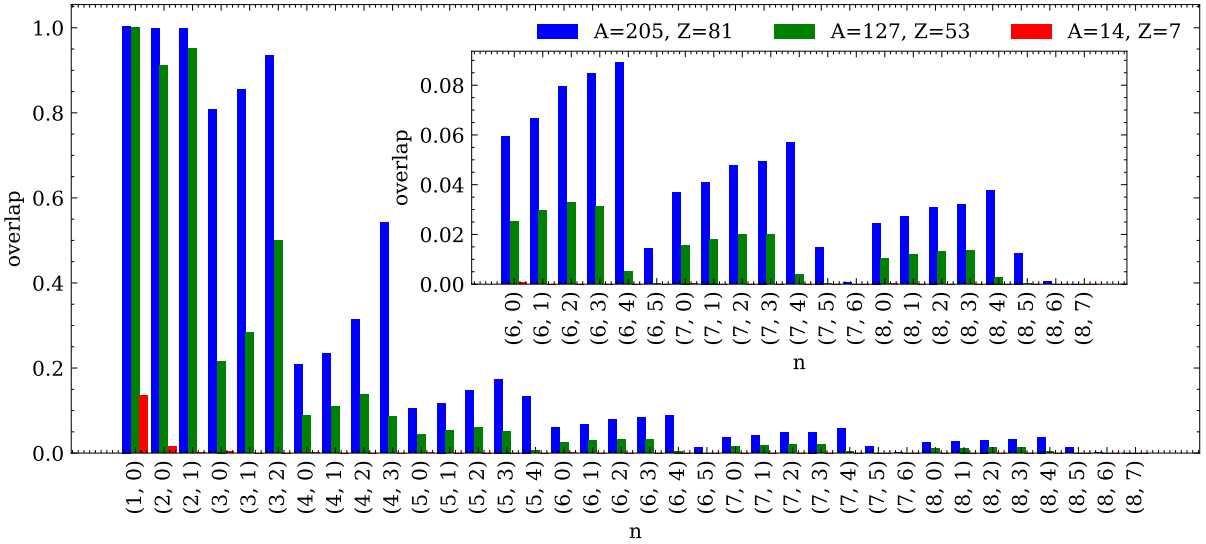

Figure 5: Wave function overlap with nucleus for different (n, l) states for iodine ($A = 127$, $Z = 53$), thallium ($A = 205$, $Z = 53$) and nitrogen ($A = 14$, $Z = 7$).

where $g_{\bar{p}}$ is g-factor of the antiproton, μ_B is Bohr magneton, m_l is magnetic quantum number and B is external magnetic field along the quantization axis [18].

The splitting between magnetic sublevels with $m_l = l$ and $m_l = -l$ is:

$$\Delta E_Z(l) = 2l\mu_B B. \tag{17}$$

Thus the ratio of Zeeman splitting (equation 17) and transition energy between n and $n-1$ energy sublevel is:

$$\frac{\Delta E_Z(l = n-1)}{\Delta E_{n,n-1}} = \frac{4(n-1)\mu_B B}{\mu Z^2}\left(\frac{1}{(n-1)^2} - \frac{1}{n^2}\right)^{-1} \tag{18}$$

Splitting to transition energy ratio as a function of n for Iodine ($A = 127$, $Z = 53$) is shown in figure 6. In case of electron shielding ($Z = 1$) Zeeman splitting is less than 2% at 5 T field compared to transition energy in a wavelength region accessible by lasers. On the other hand assuming that there is no electrons in the atom ($Z = 53$), splitting for transitions in laser accessible wavelength range is from $\approx 10\%$ to $\approx 30\%$ at 5T field. Thus energy levels are resolved at 5 T field.

3 summary

Calculations for antiprotonic atoms were carried out for transition energies, overlap of antiprotonic wave function with nucleus and Zeeman splitting for different energy levels. Calculated transition energies agree with experimental data within the stated experimental error. In case of thallium (Z=81, A=205) he greatest contribution to energy level shift comes from vacuum polarization, while finite-size effect is smaller than the experimental uncertainty.

Calculations also showed that wave function overlap first increases with angular momentum quantum number l and drops for circular states (n=l-1), which results in lower annihilation rate for circular states.

Finally Zeeman spitting was estimated to be less than 30% at 5 T field for laser accessible transitions, which means that energy levels are resolved.

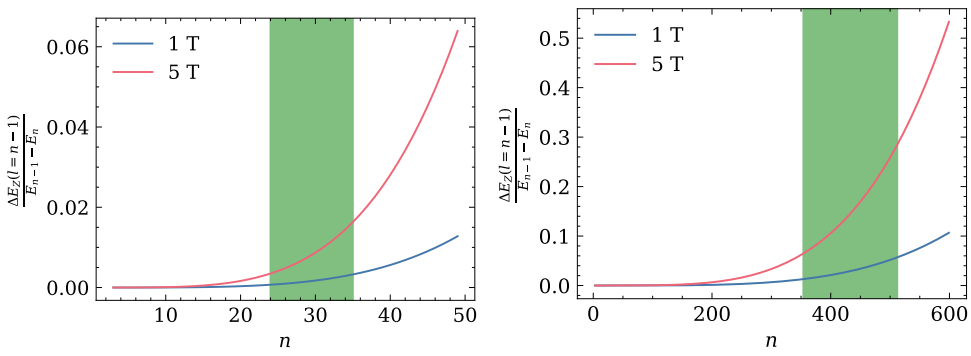

(a) Z = 1 (b) Z=53

Figure 6: Zeeman splitting and transition energy ($n+1 \to n$) ratio as a function of n for Iodine ($A = 127$, $Z = 53$) at $B = 1$ T and $B = 5$ T. Plot on the left shows splitting at $Z = 1$ assuming electron shielding and plot on the right shows splitting at $Z = 53$. Green region shows transition in a wavelength range from 1200 nm to 400 nm

Bibliography

1. Gotta, D., Rashid, K., Fricke, B., Indelicato, P. & Simons, L. X-ray transitions from antiprotonic noble gases. *The European Physical Journal D* **47,** 11–26 (2008).
2. Poth, H., Collaboration, B.-K.-S.-S.-T. & at CERN, M. C.-o. in *Physics at LEAR with Low-Energy Cooled Antiprotons* 567–588 (Springer, 1984).
3. Batty, C. Antiprotonic-hydrogen atoms. *Reports on Progress in Physics* **52,** 1165 (1989).
4. Roberson, P. *et al.* Strong interaction and mass measurements using antiprotonic atoms. *Physical Review C* **16,** 1945 (1977).
5. Rodin, V. *et al.* Low-Energy Negative Ion Injection Beamline for Experiments with Antiprotonic Atoms at AEgIS. *JACoW IPAC* **2022,** 2126–2129 (2022).
6. King, W. H. *Isotope shifts in atomic spectra* (Springer Science & Business Media, 2013).
7. Barmo, S., Pilkuhn, H. & Schlaile, H. Energy levels of light antiprotonic atoms with l>0. *Zeitschrift für Physik A Atoms and Nuclei* **301,** 283–287 (1981).
8. Ericson, T. E. O. & Scheck, F. K- nuclear interactions and yields of kaonic X-rays. *Nuclear Physics B* **19,** 450–476 (1970).
9. Backenstoss, G. *et al.* Strong interaction effects in antiprotonic atoms. *Physics Letters B* **41,** 552–556 (1972).
10. Bryan, R. & Phillips, R. Nucleon-antinucleon potential from single-meson exchanges. *Nuclear Physics B* **5,** 201–219 (1968).
11. Batty, C. Optical-model analysis of exotic atom data:(I). Kaonic atoms. *Nuclear Physics A* **372,** 418–432 (1981).
12. Von Egidy, T. Interaction and annihilation of antiprotons and nuclei. *Nature* **328,** 773–778 (1987).
13. Bamberger, A. *et al.* Observation of antiprotonic atoms. *Physics Letters B* **33,** 233–235 (1970).
14. Aramaki, T. *et al.* A measurement of atomic X-ray yields in exotic atoms and implications for an antideuteron-based dark matter search. *Astroparticle Physics* **49,** 52–62 (2013).
15. Eisenberg, Y. & Kessler, D. On the μ-mesonic atoms. *Il Nuovo Cimento (1955-1965)* **19,** 1195–1210 (1961).
16. Iljinov, A., Nazaruk, V. & Chigrinov, S. Nuclear absorption of stopped antiprotons: Multipion-nucleus interactions. *Nuclear Physics A* **382,** 378–400 (1982).
17. Wiegand, C. E. Measurement of K–mesonic x-ray spectra of medium and heavy elements. *Physical Review Letters* **22,** 1235 (1969).
18. Griffiths, D. J. & Schroeter, D. F. *Introduction to quantum mechanics* (Cambridge university press, 2018).